

1 **Effects of rotation angle and metal foam on natural convection of nanofluids in a**
2 **cavity under an adjustable magnetic field**

3 Cong Qi ^{a, b, c*}, Jinghua Tang ^{a, b}, Zi Ding ^{a, b}, Yuying Yan ^c, Leixin Guo ^{a, b}, Yifeng Ma
4 ^{a, b}

5 ^a Jiangsu Province Engineering Laboratory of High Efficient Energy Storage
6 Technology and Equipments, China University of Mining and Technology, Xuzhou
7 221116, China

8 ^b School of Electrical and Power Engineering, China University of Mining and
9 Technology, Xuzhou 221116, China

10 ^c Fluids & Thermal Engineering Research Group, Faculty of Engineering,
11 University of Nottingham, Nottingham NG7 2RD, UK

12 **Abstract:** To investigate the natural convection heat transfer of Fe₃O₄-water
13 nanofluids in a rectangular cavity under an adjustable magnetic field, two
14 experimental systems are established. Meanwhile, several factors, such as
15 nanoparticle mass fractions ($\omega=0\%$, 0.1%, 0.3%, 0.5%), magnetic field directions
16 (horizontal and vertical), magnetic field intensities ($B=0.0T$, 0.01T, 0.02T), rotation
17 angles of the cavity ($\alpha=0^\circ$, 45°, 90°, 135°), and PPI of Cu metal foam (PPI=0, 5, 15)
18 are taken into consideration to research the natural convection of Fe₃O₄-water
19 nanofluids in a rectangular cavity. With the increasing nanoparticle mass fraction,
20 Nusselt number firstly rises but then falls, and the maximum value of which appears
21 at a nanoparticle mass fraction $\omega=0.3\%$. Horizontal magnetic field is not significant to
22 the thermal performance enhancement, but vertical magnetic field shows an opposite
23 trend and makes a positive contribution to the thermal performance. The cavity with a
24 rotation angle $\alpha=90^\circ$ shows the highest thermal performance. Nusselt number of the
25 cavity filled with metal foam can be improved obviously compared with that without
26 metal foam. But the increasing PPI of metal foam is disadvantageous to heat transfer

*Correspondence author.

E-mail: qicong@cumt.edu.cn (C. Qi); tangjh@cumt.edu.cn (J. Tang); edu_dingzi@163.com (Z. Ding); yuying.yan@nottingham.ac.uk (Y. Yan); guoleixin@cumt.edu.cn (L. Guo); myf@cumt.edu.cn (Y. Ma)

27 performance.

28 **Key words:** Nanofluids; Natural convection; Magnetic field; Metal foam

29	Nomenclature	55	
30	A	cross-sectional area, m^2	56 T_H^*
31	c_p	specific heat of nanofluids,	57
32		$J \cdot kg^{-1} \cdot K^{-1}$	58 T_H
33	E	heat transfer enhancemental	59
34		ratio	60 T_{in}
35	h	convective heat transfer	61 T_m
36		coefficient, $W \cdot m^{-2} \cdot K^{-1}$	62
37	I	electric current, A	63 T_{out}
38	l	width of cavity, m	64 U
39	Nu	Nusselt number of nanofluids	65
40	q_m	mass flow rate, $kg \cdot s^{-1}$	66 Greek symbols
41	Q	heating power, W	67 α
42	Q_{loss}	heat loss, W	68 ω
43	Q'_{net}	effective heat absorption for	69 δ
44		nanofluids, W	70 λ_w
45	Q''_{net}	effective heat absorption for	71
46		water, W	72 λ_f
47	Q_{net}	average effective heat	73
48		absorption, W	74
49	T_C	inside surface (cold side)	75 Subscripts
50		temperature of left cavity, K	76 C
51	T_C^*	outside surface (cold side)	77 f
52		temperature of right cavity, K	78 H
53	T'_C	inside surface (cold side)	79 w
54		temperature of right cavity, K	

80

81

82

83

84

85

86

87

88

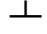
89 **1 Introduction**

90 Since the conception of nanofluids was put forward, many scholars have
91 prepared many kinds of nanofluids and researched their thermophysical parameters
92 and thermal performance [1, 2]. It is found that nanofluids are far superior to
93 common fluids in terms of heat conduction. Therefore, nanofluids have been used in
94 various fields, for example, photothermal conversion [3, 4], thermal management of
95 electronics [5, 6, 7], phase change heat transfer [8, 9, 10, 11], heat storage unit with
96 fins [12, 13], tubes with combined turbulator [14], forced convection in
97 heat exchanger system including external thread tubes with built-in twisted belt [15,
98 16], tubes with double twisted tapes [17], triangle tubes with built-in twisted belt
99 [18], double tube heat exchanger with tape insert material [19], a cylindrical
100 enclosure [20], porous media [21, 22, 23], helically corrugated tube [24], and
101 micro-channel heat sink [25, 26]. Some reviews on the other applications of
102 nanofluids can be also obtained from Babar et al. [27].

103 For natural convection, many investigations have been carried out by scientists
104 because of its safety and quietness. Sheikholeslami et al. have done a variety of
105 researches on natural convection of nanofluids. Such as, natural convection of
106 nanofluids in a porous enclosure with applied electric field [28], a porous media with
107 applied electric field based on CVFEM [29], a circular enclosure with melting
108 surface under magnetic field [30], a porous enclosure using non-equilibrium model
109 [31], a permeable medium via Darcy law [32], a porous enclosure considering the
110 thermal radiation and Coulomb force [33], a permeable media under external

111 magnetic source [34], a porous complex shaped cavity based on thermal radiation
112 [35], a permeable medium by an innovative computer method [36], and a circular
113 cavity under the variable magnetic forces [37]. Izadi et al. analyzed the natural
114 convection in a porous gap under a variable magnetic field [38], and the natural
115 convection in a porous medium filled with multi-walled carbon
116 nanotube-Fe₃O₄/water magnetic hybrid nanofluids [39]. Not only are the effect of
117 Hartmann number on the thermal performance discussed in above references, but as
118 well as Darcy number and Rayleigh number. From above references, the relationship
119 between thermal performance and Darcy number, Hartmann number, Rayleigh
120 number can be discovered, which shows that Hartmann number can reduce the heat
121 transfer rate, but Darcy and Rayleigh number are beneficial to the improvement of
122 temperature gradient.

123 Pordanjani et al. [40] analyzed the entropy generation of nanofluids' natural
124 convection in an inclined square cavity under a magnetic field. Results indicated that
125 thermal performance can be improved by the increase of magnetic field angle from 0 °
126 to 45 °. Pordanjani et al. [41] designed an enclosure with sinusoidal wall temperature
127 distribution and investigated the natural convection of nanofluids under magnetic
128 field. Results showed that Nusselt number is proportional to magnetic field angle
129 and Rayleigh number, but deteriorates with the increase of aspect ratio and
130 Hartmann number.

131 Izadi et al. used LBM to explore the natural convection of a T-shaped enclosure
132 [42] and  shaped cavity [43] which is full of nanofluids, between two eccentric

133 cylinders filled with porous material based on Buongiorno's two phase model [44],
134 inside a porous enclosure with undulant-wall by LTNE and two-phase model [45],
135 inside a porous enclosure under variable magnetic fields [46], and in a C-shaped
136 cavity by LBM [47]. Xu et al. [48] also applied LBM to study the effects of porous
137 foam on the natural convection transport of nanofluids in a cavity. The results of
138 above studies presented that the thermal performance can be improved by
139 augmenting the heat source aspect ratio, Rayleigh number, porosity and magnetic
140 strength while deteriorates with Lewis number.

141 Safaei et al. simulated the natural convection of a shallow cavity full of
142 nanofluids while taking thermal radiation into consideration [49], an incinerator with
143 a hot block [50], and cavities with different aspect ratios [51]. Zhou et al. not only
144 numerically explored the natural convection of liquid-metal nanofluids in a cavity
145 [52], around a bubble in a cavity [53], but also researched the surface tension driven
146 convection in a rectangular cavity [54]. Results showed that Rayleigh number,
147 Grashof number, emissivity, height and width of heater can all improve the heat
148 transfer, while Hartmann number can worsen it.

149 Mehryan et al. [55] explored the natural convection of nanofluids in a square
150 enclosure under a periodic magnetic field. Results revealed that the period of
151 magnetic field can argument the heat transfer and entropy generation. Sheremet et al.
152 researched the natural convection of a baffled U-shaped cavity full of nanofluids
153 [56], an inclined cavity with time-periodic temperature boundary [57], an open
154 cavity including multiple porous layers [58], an open cavity containing a

155 heat-generating element [59, 60] and an open triangular cavity considering the
156 Brownian diffusion [61]. Selimefendigil et al. discussed the natural convection of
157 nanofluids in various cavities, such as, a three-dimensional cavity containing two
158 adiabatic inner rotating cylinders [62], a cavity filled with CNT-water nanofluids
159 [63], a 3D trapezoidal cavity [64], a lid-driven trapezoidal cavity [65], and a cubic
160 enclosure including an inner rotating cylinder [66]. Mohebbi et al. [67] introduced
161 the natural convection in a Γ -shaped enclosure full of nanofluids. Sajjadi et al. [68]
162 and Mohebbi et al. [69] analyzed the natural convection of nanofluids in a porous
163 media. Above studies analyzed the effect of boundary temperature oscillating
164 frequency, Rayleigh number, nanoparticle concentration, porous medium on heat
165 transfer, all of which can be instrumental in enhancing heat transfer. Qi et al. [70, 71]
166 used LBM to simulate the influence of nanoparticle size on natural convection. The
167 mechanism for heat transfer enhancement is revealed that the Brown force is the
168 main factor in contrast to other forces.

169 Above references mainly discussed the various shape cavities filled with
170 nanofluids. However, effects of rotation angle on the natural convection of
171 nanofluids under different magnetic field directions and intensities are less
172 investigated, and the influence of metal foam PPI under different magnetic field
173 directions and intensities are also less investigated. Hence, the purpose of this study
174 is to experimentally reveal the effects of rotation angle and metal foam on natural
175 convection of nanofluids in a cavity under an adjustable magnetic field direction and
176 intensity.

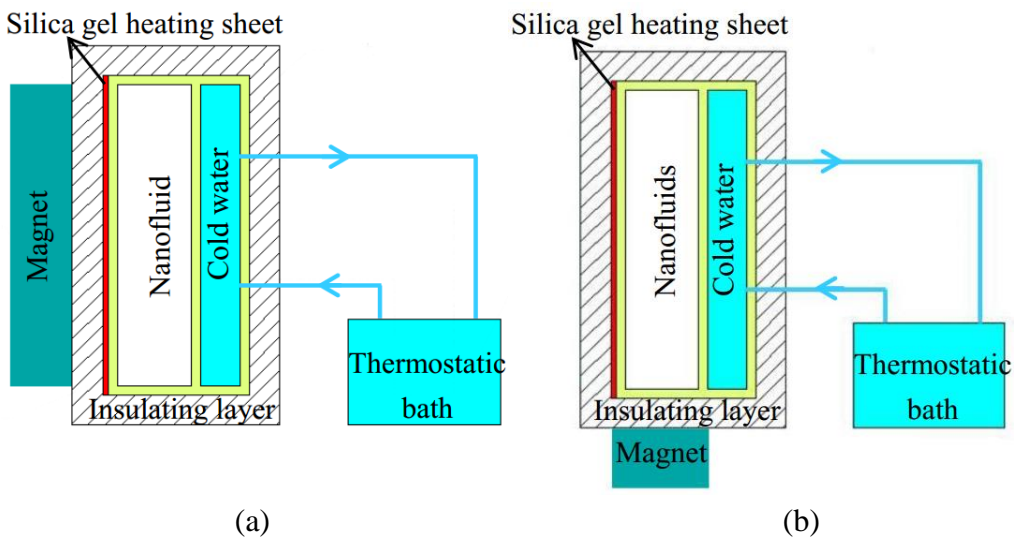
177 2 Method

178 2.1 Experimental system

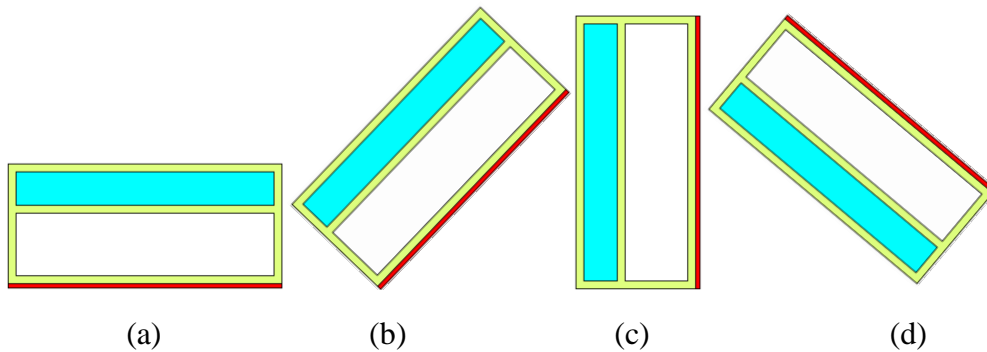
179 2.1.1 Effect of rotation angles

180 An experiment is designed to study the natural convection performance of a
181 rectangular cavity filled with Fe₃O₄-water nanofluids under different magnetic fields.
182 Fe₃O₄ nanofluids belong to magnetofluid, and the influence of magnetic fields on
183 magnetofluid is larger than other nanofluids. In addition, compared with other base
184 liquids, water is cheaper and easier to obtain. Hence, water and Fe₃O₄ are chosen as
185 the base fluid and nanoparticles in this experiment. Considering the Fe₃O₄-water
186 nanofluids are mainly affected by the Lorentz force under the induced magnetic field,
187 different magnetic field intensities are considered and B is employed to refer to the
188 magnetic field intensity of the induced magnetic field. Hence, Effects of several
189 factors, such as nanoparticle mass fractions ($\omega=0\%$, 0.1%, 0.3%, 0.5%), magnetic
190 field directions (horizontal (rightward) and vertical (downward)), magnetic field
191 intensities ($B=0.01\text{T}$, 0.02T) and rotation angles ($\alpha=0^\circ$, 45° , 90° , 135°), on the
192 thermal performance are analyzed. The schematic diagram of natural convection
193 system without metal foam is demonstrated in Fig. 1. The size of the left cavity is
194 100 mm (length) \times 100 mm (height) \times 25mm (width), which is filled with nanofluids.
195 The material of the cavity is made of copper, and the thickness of the copper is 5mm.
196 The cold water flows through the right small cavity to keep the right wall (cold side)
197 of the left cavity at a low constant temperature. A silica gel heating sheet ($Q=15\text{W}$) is
198 used to provide a high constant temperature for the left wall (hot side) of the left

199 cavity. A magnet attached to the left and bottom wall is applied to supply a
 200 horizontal magnetic field and vertical magnetic field respectively, and Gauss meter
 201 (CH-15, errors: $\pm 1\text{G}$) is used to measure the magnetic intensity. Insulation, the
 202 material of which is composed of silicic acid rock wool and foam sponge, is adopted
 203 to reduce the heat loss. A thermostatic bath (DC-2030, errors: $\pm 0.02^\circ\text{C}$) is employed
 204 to offer the low constant temperature water. The temperature of import and export of
 205 the cold fluid and outside surface temperature of the left cavity can be measured by
 206 the thermocouples (T type, range: $0\sim 200^\circ\text{C}$). Then, data will be collected by a data
 207 acquisition instrument (34970, channels: 22). The details of the different rotation



208
 209 (a) (b)
 210 Fig. 1. Schematic diagram of free convection system without metal foam, (a)
 211 horizontal (rightward) magnetic field, (b) vertical (downward) magnetic field

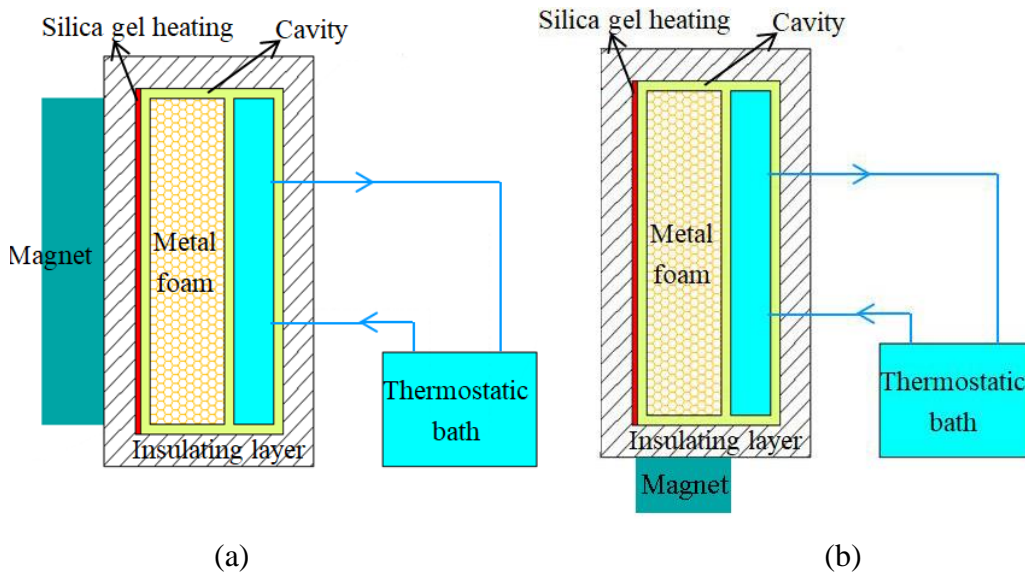


212
 213 (a) (b) (c) (d)
 214 Fig. 2. Details of the different rotation angles, (a) $\alpha=0^\circ$; (b) $\alpha=45^\circ$; (c) $\alpha=90^\circ$; (d)
 215 $\alpha=135^\circ$

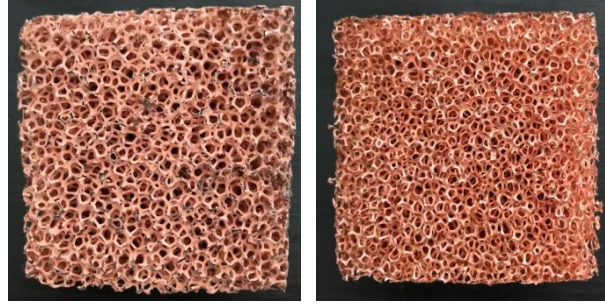
216 angles ($\alpha=0^\circ, 45^\circ, 90^\circ, 135^\circ$) are presented in Fig. 2.

217 2.1.2 Effect of metal foam

218 Based on the corresponding rotation angle for the highest thermal performance
219 of section "2.1.1 Effect of rotation angles ", Cu metal foam is filled in the cavity with
220 the best rotation angle to augment the heat transfer. And the effects of nanoparticle
221 mass fractions ($\omega=0\%, 0.1\%, 0.3\%, 0.5\%$), magnetic field directions (horizontal and
222 vertical) and magnetic field intensities ($B=0.01T, 0.02T$), the influence of PPI (PPI=5,
223 15) on the natural convection are also investigated. Fig. 3 presents the schematic
224 diagram of natural convection system with metal foam. The detail of Cu metal foam
225 with different PPI (PPI=5, 15) are given in Fig. 4. And their structural parameters are
226 presented in Table 1.



229 Fig. 3. Schematic diagram of free convection system with metal foam, (a) horizontal
230 (rightward) magnetic field, (b) vertical (downward) magnetic field



(a)

(b)

Fig. 4. Metal foam with different PPI, (a) PPI=5, (b) PPI=15

Table 1 Structural parameters of metal foam

NO	PPI	Porosity	Bore diameter (mm)
1	5	94.08%	0.81
2	15	94.08%	0.57

231

232

233

234

235 2.2 Data processing

236 Calculation of the volume fraction of nanofluids is as follows:

$$237 \quad \varphi = \frac{1}{(1/\omega)(\rho_f/\rho_n)} \quad (1)$$

238 Heating power of DC power is as follows:

$$239 \quad Q = UI \quad (2)$$

240 Effective heat absorption of hot fluid (nanofluids) is as follows:

$$241 \quad Q'_{\text{net}} = Q - Q_{\text{loss}} \quad (3)$$

242 where, the Q_{loss} is measured by a heat flow meter.

243 Effective heat absorption can be also calculated from the cold fluid (water):

$$244 \quad Q''_{\text{net}} = c_p q_m (T_{\text{out}} - T_{\text{in}}) \quad (4)$$

245 Average effective heat absorption is chosen in the experiment:

$$246 \quad Q_{\text{net}} = \frac{Q'_{\text{net}} + Q''_{\text{net}}}{2} \quad (5)$$

247 Outside surface (hot side) temperature of the left cavity is calculated by the

248 following formula:

$$249 \quad T_H^* = \frac{(T_1 + T_2 + \dots + T_6)}{6} \quad (6)$$

250 Inside surface (hot side) temperature of the left cavity is calculated by the
251 following formula:

$$252 \quad T_H = T_H^* - \frac{Q_{net} \delta}{A \lambda_w} \quad (7)$$

253 Also, outside surface (cold side) temperature of the right cavity is calculated by
254 the following formula:

$$255 \quad T_C^* = \frac{(T_7 + T_8 + \dots + T_{12})}{6} \quad (8)$$

256 Inside surface (cold side) temperature of the right cavity is as follows:

$$257 \quad T_C' = T_C^* - \frac{Q_{net} \delta}{A \lambda_w} \quad (9)$$

258 The temperature of cold water in the right cavity is constant, and the
259 temperature of cold water is the same with the inner surface temperature on both
260 sides of the right cavity respectively. Hence, the inside surface (cold side)
261 temperature of the left cavity can be obtained from the following form:

$$262 \quad T_C = T_C^* - \frac{2Q_{net} \delta}{A \lambda_w} \quad (10)$$

263 Qualitative temperature of the nanofluids in the left cavity is as follows:

$$264 \quad T_m = \frac{T_H + T_C}{2} \quad (11)$$

265 Calculation of convective heat transfer coefficient is as follows:

$$266 \quad h = \frac{Q_{net}}{A(T_H - T_C)} \quad (12)$$

267 Nusselt number is defined as:

268
$$Nu = \frac{h \cdot l}{\lambda_f} \quad (13)$$

269 Heat transfer enhancement ratio is calculated by following formula:

270
$$E = \frac{Nu - Nu_{(0.0\%+PPI=0)}}{Nu_{(0.0\%+PPI=0)}} \quad (14)$$

271 **2.3 Uncertainty analysis**

272 Error transfer formula for Nusselt number can be obtained from [72]:

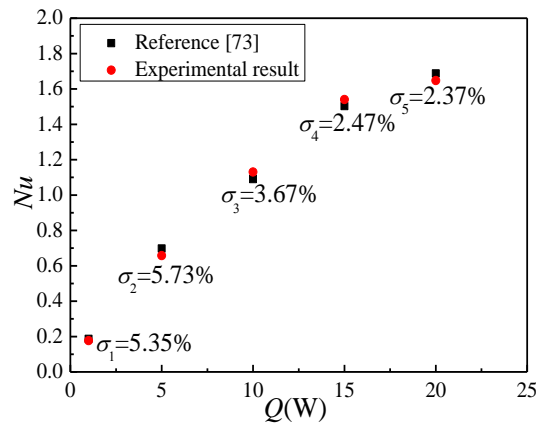
273
$$\frac{\Delta Nu}{Nu} = \left| \frac{\partial \ln Nu}{\partial h} \right| \Delta h + \left| \frac{\partial \ln Nu}{\partial W} \right| \Delta W + \left| \frac{\partial \ln Nu}{\partial \lambda_f} \right| \Delta \lambda_f =$$

$$\frac{\Delta h}{h} + \frac{\Delta W}{W} + \frac{\Delta \lambda_f}{\lambda_f} \quad (15)$$

274 The errors of the Nusselt number can be calculated from equation (15) and it is
 275 only 6.34% in this experiment, which guarantees the dependability of the
 276 experimental system.

277 **2.4 Experimental verification**

278 Experimental verification cannot be neglected to ensure the accuracy of this
 279 experiment. The results of water in the cavity are compared with that of other
 280 reference [73], and it is illustrated in Fig. 5. It can be found that they are close to



281
 282 Fig. 5. Comparison of Nusselt numbers between experimental data and
 283 literature values [73]

284

285 each other, and the max error is only 5.73%, which explains that the experimental set
286 has a high accuracy.

287 **3 Results and discussions**

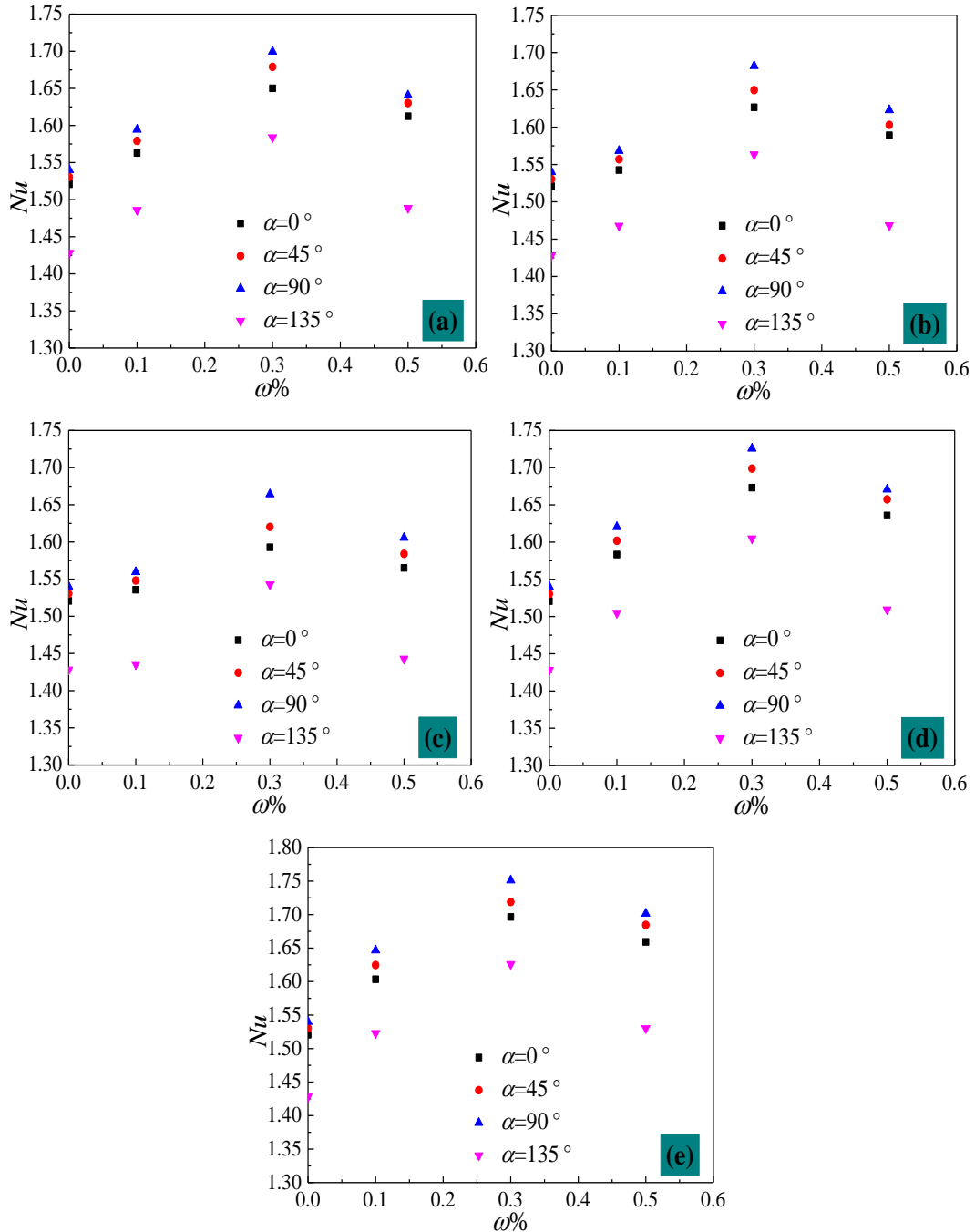
288 3.1 Effect of rotation angles

289 For the cavity without metal foam, relationships between rotation angles and
290 Nusselt number under different magnetic field directions and intensity are researched,
291 whose results are showed in Fig. 6. In Fig. 6, nanofluids with mass fractions of 0.1%,
292 0.3% and 0.5% correspond to nanofluids with volume concentration of 0.019%,
293 0.058% and 0.097%, respectively. If the concentration is too low, the heat transfer
294 can hardly be enhanced. However, the agglomeration trend of nanoparticles will
295 increase with the increasing concentration of nanoparticles, which will result in the
296 weakening of the stability of nanofluids. To ensure the stability and high thermal
297 conductivity of nanofluids, nanofluids with volume concentration of 0.019%, 0.058%
298 and 0.097% are selected. And results indicate that Nusselt number rises with the
299 nanoparticle mass fraction firstly and then falls. The critical nanoparticle mass
300 fraction $\omega=0.3\%$ can be got due to its highest Nusselt number. As we know, there are
301 three important factors (heat conductivity, viscosity, Brownian motion of
302 nanoparticles) playing the largest role on heat transfer enhancement. A thermal
303 conductivity measuring instrument (model: DRE-III, accuracy: $\pm 2-3\%$) is applied
304 to obtain the thermal conductivity and a viscosity meter (model: NDJ-8S, accuracy:
305 $\pm 2\%$) is used to measure the viscosity in this experiment. The detail results can be
306 found in our previous published paper [74]. As the increasing of nanoparticles

307 concentration, the heat transfer performance of nanofluids will be enhanced not only
308 because of its higher thermal conductivity caused by nanoparticles, but also due to
309 the large turbulivity induced by the Brownian motion of nanoparticles. However, as
310 the concentration of nanoparticles increases, viscosity also increases, which can
311 cause a reduction in heat transfer performance. When nanoparticle mass fraction is
312 lower than $\omega=0.3\%$, high heat conductivity and Brownian motion are major roles on
313 Nusselt number. However, when nanoparticle mass fraction is larger than $\omega=0.3\%$,
314 the viscosity becomes to play a more crucial role instead of the heat conductivity and
315 Brownian motion of nanoparticles. So the mass fraction of nanoparticles $\omega=0.3\%$
316 becomes the corresponding critical concentration of nanoparticles with the highest
317 Nusselt number.

318 Another important conclusion is obtained that the cavity with a rotation angle
319 $\alpha=90^\circ$ shows the best thermal performance, followed by $\alpha=45^\circ$ and $\alpha=0^\circ$, and the
320 cavity with a rotation angle $\alpha=135^\circ$ behaves the worst thermal performance. Fig. 7
321 presents the influence of rotation angles on the relative heat transfer enhancement
322 ratio compared with the worst working condition. It is found that Nusselt number
323 enhancement ratio is proportional to rotation angle (from $\alpha=0^\circ$ to $\alpha=90^\circ$), and the
324 enhancement ratio of cavity with $\alpha=90^\circ$ can reach 11.29% at best. For the cavity
325 with $\alpha=135^\circ$, the hot side locates in the top and the cold side locates in the bottom.
326 Fluid near the top hot side is heated and moves upward, but fluid near the bottom
327 cold side is cooled and moves downward, and the top and bottom walls prevent the
328 flow. Hence, natural convection becomes weak, and heat conduction plays a major

329 role in this condition. Therefore, the cavity with $\alpha=135^\circ$ shows the worst thermal
 330 performance. For cavity with $\alpha=0^\circ$, the hot side locates in the bottom and cold side
 331 locates in the top. Fluid near the bottom is heated and flows upward and fluid near



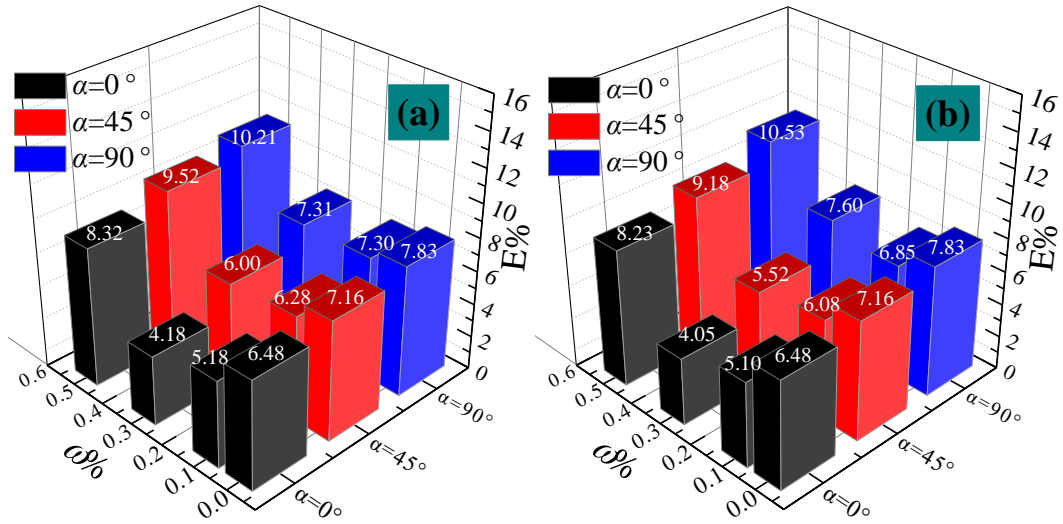
332

333

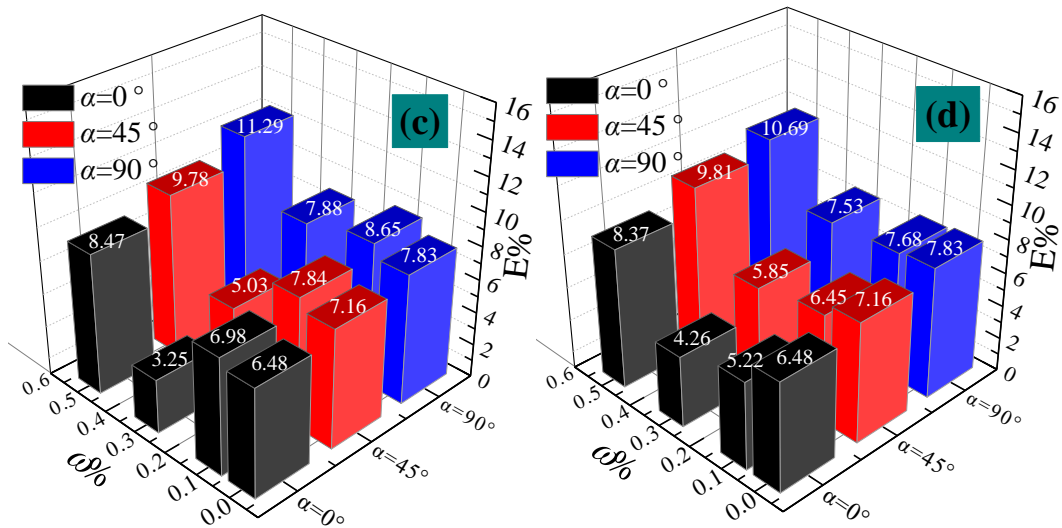
334

335 Fig. 6. Effects of rotation angles on Nusselt number under different magnetic fields,
 336 (a) no magnetic field, (b) horizontal magnetic field with $B=0.01T$, (c) horizontal
 337 magnetic field with $B=0.02T$, (d) vertical magnetic field with $B=0.01T$, (e) vertical
 338 magnetic field with $B=0.02T$

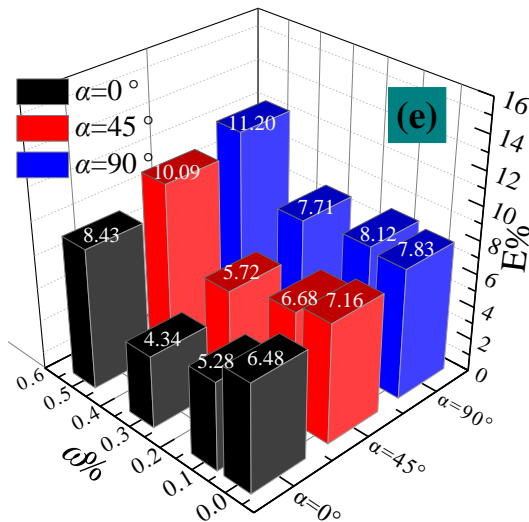
339



340



341



342

343

Fig. 7. Effects of rotation angles on Nusselt number enhancement ratio compared with that with $\alpha=135^\circ$ at the same condition, (a) no magnetic field, (b) horizontal magnetic field with $B=0.01\text{T}$, (c) horizontal magnetic field with $B=0.02\text{T}$, (d) vertical magnetic field with $B=0.01\text{T}$, (e) vertical magnetic field with $B=0.02\text{T}$

346

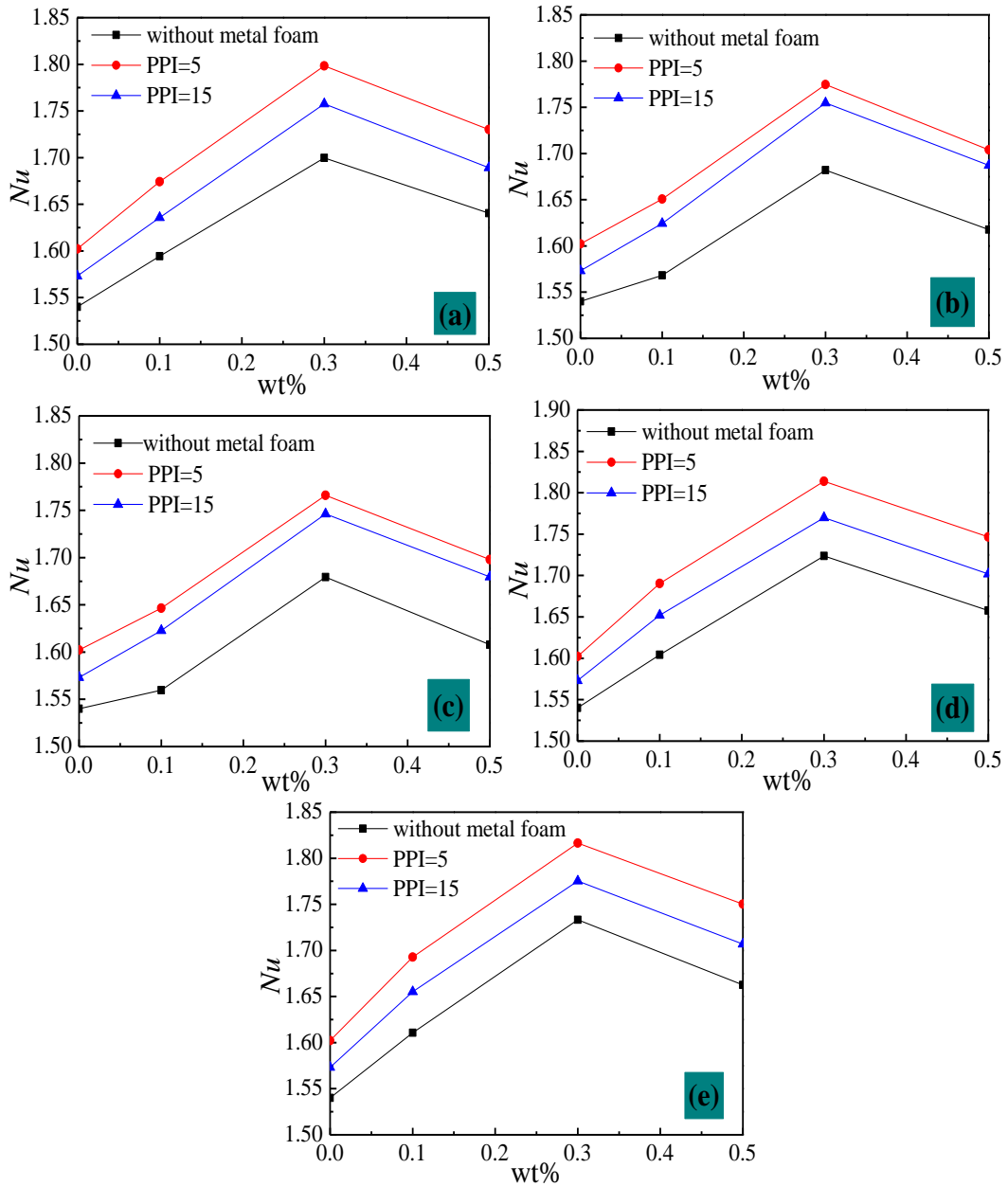
347

348 the top is cooled and flows downward. Besides, hot and cold fluids flow in opposite
349 directions, which is also disadvantageous to the increase of natural convection.
350 Hence, the thermal performance of cavity with $\alpha=0^\circ$ is much lower than that with
351 $\alpha=90^\circ$ but is better than the cavity with $\alpha=135^\circ$ which is mainly heat conduction.
352 The cavity with a rotation angle $\alpha=45^\circ$ is between $\alpha=90^\circ$ and $\alpha=0^\circ$, and its thermal
353 performance is also between them.

354 3.2 Effect of PPI

355 From the results in above section, it can be obtained that the cavity with a
356 rotation angle $\alpha=90^\circ$ reveals the best thermal performance. So as to improve the
357 natural convection further, Cu metal foam is filled in the cavity with a rotation angle
358 $\alpha=90^\circ$. The experimental system can be found in Fig. 3. Effects of PPI (PPI=5, 15)
359 of Cu metal foam on Nusselt number under different direction and intensity
360 magnetic fields are given in Fig. 8. Results indicate that metal foam is significant in
361 the heat transfer of cavity, the maximum value of Nusselt number can be got when
362 PPI=5 and $\omega=0.3\%$. In porous media, there are two main heat transfer models
363 including convection heat transfer and heat conduction. For metal foam with PPI=5,
364 convection heat transfer dominates the major role in heat transfer. As the increase
365 from PPI=5 to PPI=15, the flow of fluid is blocked and the heat transfer is weakened,
366 so convection heat transfer begins to deteriorate badly although the role of heat
367 conduction increases. As the increase of nanoparticle mass fraction from $\omega=0.0\%$ to
368 $\omega=0.3\%$, convection is improved due to the high thermal conductivity of
369 nanoparticles. However, as the increase of nanoparticle mass fraction from $\omega=0.3\%$

370 to $\omega=0.5\%$, there is a large increase in viscosity which causes a deterioration in heat
371 transfer. Effects of PPI on Nusselt number enhancement ratio are presented in Fig. 9.
372 It shows that Nusselt number of cavity with PPI=5 and PPI=15 metal foam without
373 magnetic field can be improved by 5.81% and 3.41% at best when compared with
374 the data without metal foam respectively. Cavity with PPI=5, PPI=15 metal foam can
375 improve the heat transfer by 5.60%, 4.47% under horizontal magnetic field and
376 5.36%, 2.97% under vertical magnetic field at best compared with the cavity without
377 metal foam respectively. As we know, there are two important factors affecting the
378 thermal performance, one is the high heat conductivity of metal foam which can
379 enhance the whole heat conductivity of the cavity, and another is the porous shape
380 which can increase the disturbance in the cavity. From Table 1, it is found that the
381 porosities of these two metal foams are the same, which means that the amount of
382 metal foam is the same. Hence, the two kinds of metal foam make the same
383 contribution to the whole heat conductivity enhancement of the whole cavity.
384 However, convection heat transfer is more intense as the increasing pore size
385 (decreasing PPI) at the same porosity. Compared with the cavity with PPI=15 metal
386 foam, convective heat transfer occupies a larger proportion in the cavity with PPI=5
387 metal foam. Therefore, Nusselt number is inversely proportional to PPI.



388

389

390

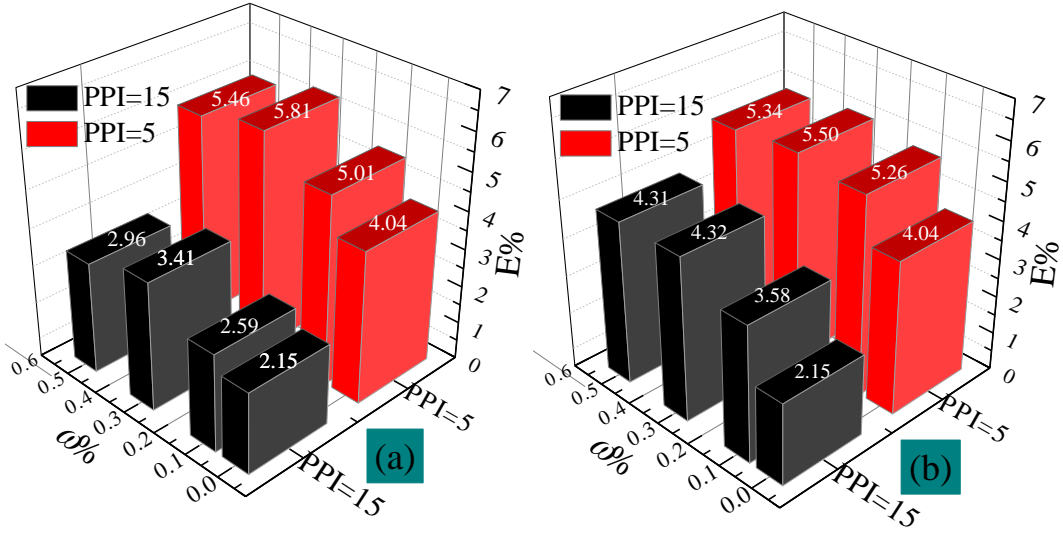
391

392

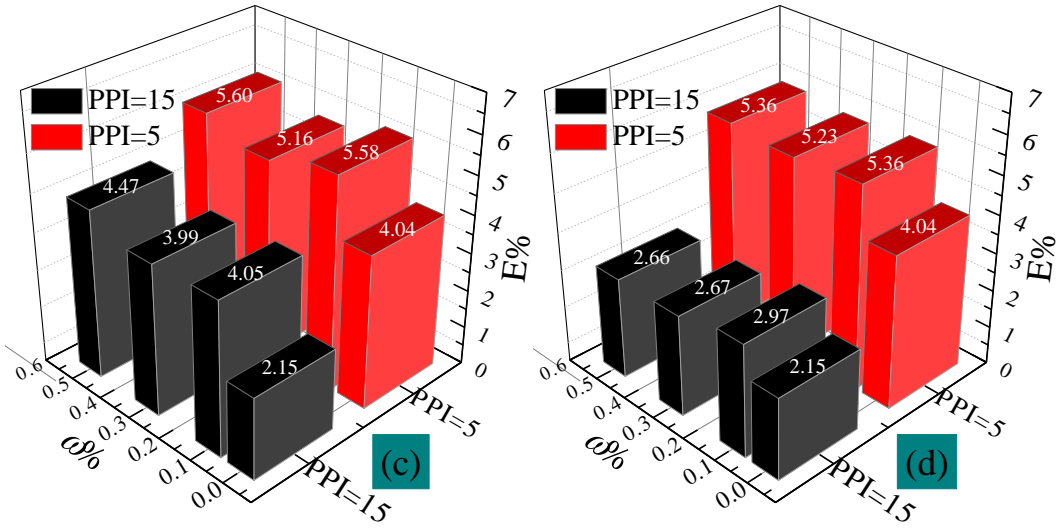
393

394

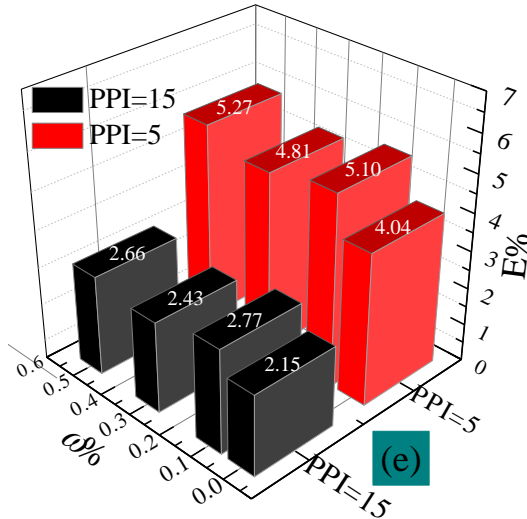
Fig. 8. Effects of PPI on Nusselt number under different magnetic fields, (a) no magnetic field, (b) horizontal magnetic field with $B=0.01T$, (c) horizontal magnetic field with $B=0.02T$, (d) vertical magnetic field with $B=0.01T$, (e) vertical magnetic field with $B=0.02T$



395



396



397

398

399

400

401

402

Fig. 9. Effects of PPI on Nusselt number enhancement ratio compared with that without metal foam at the same condition, (a) no magnetic field, (b) horizontal magnetic field with $B=0.01T$, (c) horizontal magnetic field with $B=0.02T$, (d) vertical magnetic field with $B=0.01T$, (e) vertical magnetic field with $B=0.02T$

403 3.3 Effect of magnetic fields

404 Also, effects of magnetic field direction and intensity on Nusselt number at
 405 different PPI are discussed, which are shown in Fig. 10. Results indicate that
 406 horizontal magnetic field can reduce the natural convection of nanofluids in the
 407 cavity, but vertical magnetic field can improve the natural convection. Higher
 408 horizontal magnetic field intensity can cause smaller Nusselt number, and higher
 409 vertical magnetic field intensity can cause larger Nusselt number.

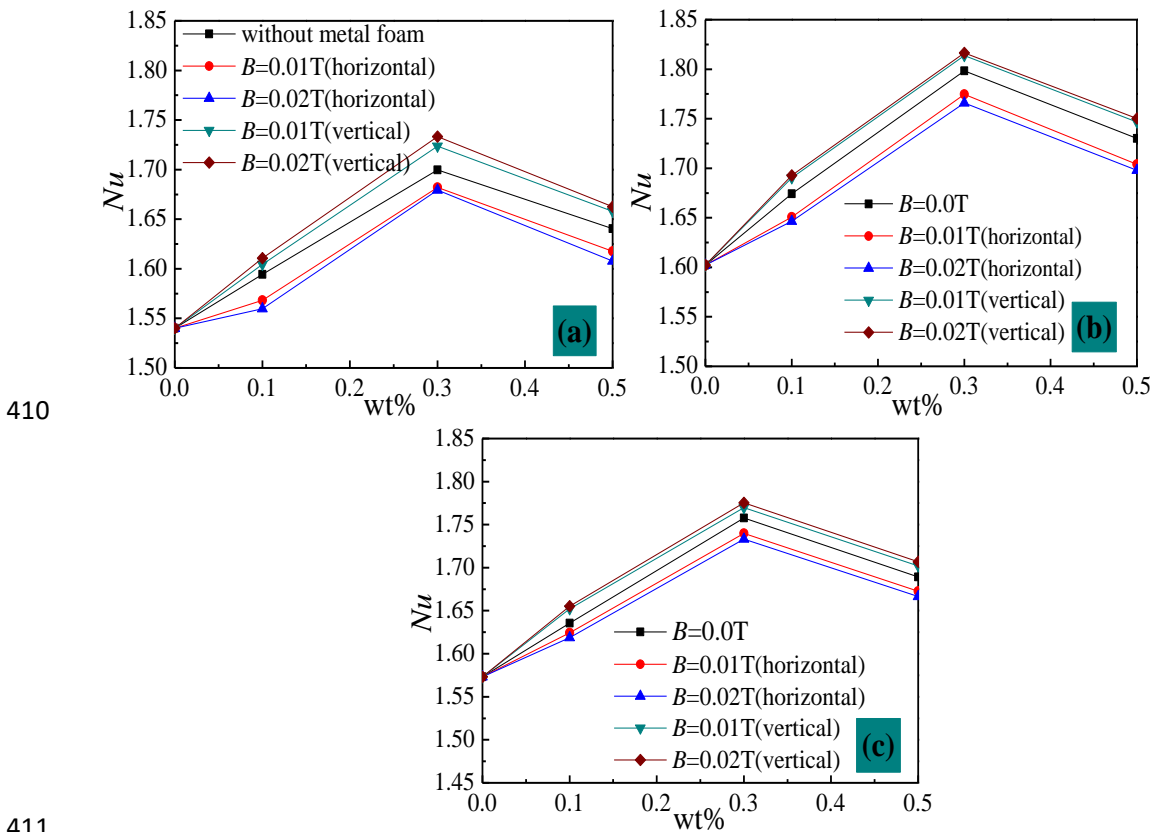
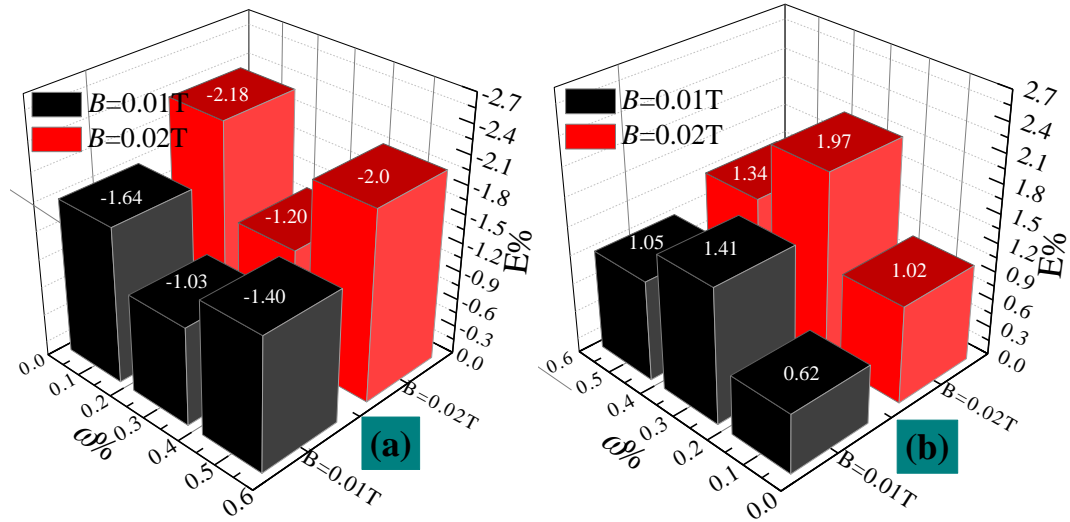
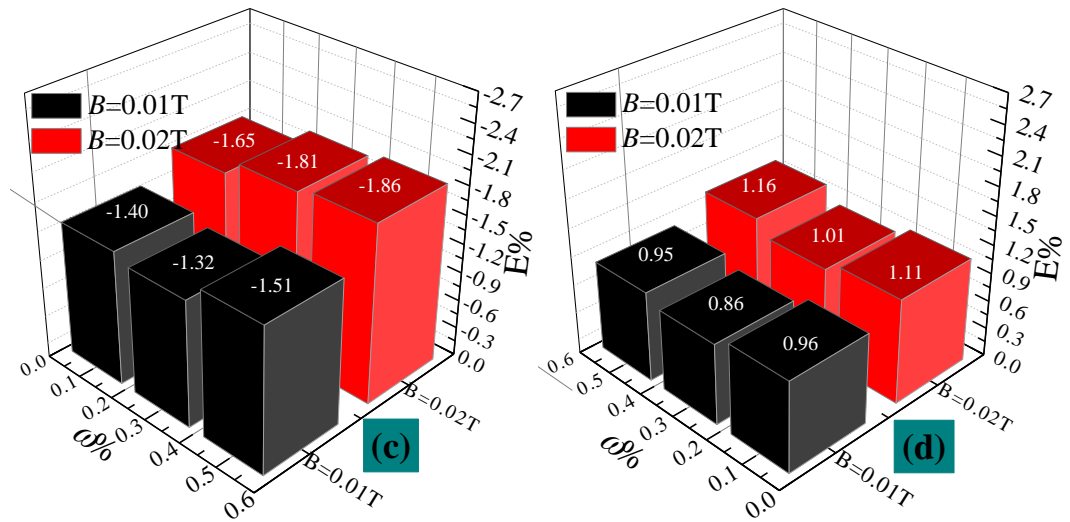


Fig. 10. Effects of magnetic field on Nusselt number at different PPI, (a) without metal foam, (b) PPI=5, (c) PPI=15

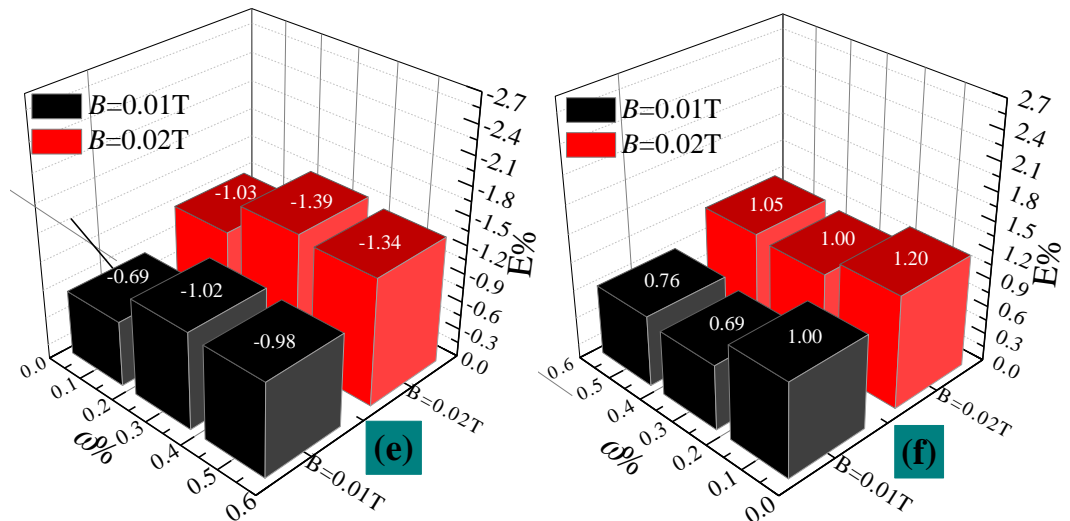
414 Effects of magnetic field on Nusselt number enhancement ratio are presented in
 415 Fig. 11. Results display that horizontal magnetic field can reduce the natural
 416 convection without metal foam by 2.18% at best, and vertical magnetic field can
 417 enhance the natural convection without metal foam by 1.97% at best. Also, results



418



419



420

421

422

423

424

425

Fig. 11. Effects of magnetic field on Nusselt number enhancement ratio compared with that without magnetic field, without metal foam: (a) horizontal magnetic field, (b) vertical magnetic field, PPI=5: (c) horizontal magnetic field, (d) vertical magnetic field, PPI=15: (e) horizontal magnetic field, (f) vertical magnetic field

426 show that horizontal magnetic field can reduce the natural convection with metal
427 foam by 1.86% at best, and vertical magnetic field can enhance the natural
428 convection with metal foam by 1.20% at best. The resultant force direction of
429 horizontal (rightward) magnetic field force and gravity force is bottom right, which
430 is equivalent to the physical model of hot side on top and cold side on bottom.
431 However, above physical model is disadvantageous to natural convection but it is
432 to the benefit of heat conduction. Hence, the horizontal (rightward) magnetic field
433 can reduce the natural convection. For the vertical (downward) magnetic field, the
434 resultant force direction of vertical (downward) magnetic field force and gravity
435 force is the same with that of gravity force, which is equivalent to the physical model
436 of larger gravity force. Larger gravity force can make positive contribution to the
437 enhancement of natural convection. Therefore, vertical (downward) magnetic field
438 can increase the natural convection.

439 **4 Conclusions**

440 An experiment system is set to study the effects of rotation angle and metal
441 foam on natural convection of nanofluids in the cavity under an adjustable magnetic
442 field. Relevant conclusions are obtained as follows:

443 (1) Cavity with a rotation angle $\alpha=90^\circ$ shows the best thermal effect, followed
444 by $\alpha=45^\circ$ and $\alpha=0^\circ$, and the cavity with a rotation angle $\alpha=135^\circ$ behaves the worst
445 thermal performance. Nusselt number of cavity with $\alpha=90^\circ$ is enhanced by 11.29%
446 at highest in comparison with that with a rotation angle $\alpha=135^\circ$.

447 (2) Natural convection heat transfer rises with nanoparticle mass fraction (from

448 $\omega=0.0\%$ to 0.3%) firstly but then falls (from $\omega=0.3\%$ to $\omega=0.5\%$). Nanofluids with a
449 critical nanoparticle mass fraction $\omega=0.3\%$ shows the highest Nusselt number.

450 (3) Metal foam is significant in the heat transfer of cavity, as the increase of PPI,
451 the Nusselt number decreases.

452 (4) Horizontal magnetic field can reduce the natural convection of nanofluids in
453 the cavity, but vertical direction of it can improve the natural convection. Higher
454 horizontal magnetic field intensity can cause smaller Nusselt number, and higher
455 vertical magnetic field intensity can cause larger Nusselt number.

456 **Acknowledgements**

457 This work is financially supported by "National Natural Science Foundation of
458 China" (Grant No. 51606214), "Natural Science Foundation of Jiangsu Province,
459 China" (Grant No. BK20181359) and "EU ThermaSMART project,
460 H2020-MSCA-RISE (778104)-Smart thermal management of high power
461 microprocessors using phase-change (ThermaSMART)".

462 **References**

- 463 [1] M.H. Esfe, S. Esfandeh, M.K. Amiri, M. Afrand, A novel applicable
464 experimental study on the thermal behavior of SWCNTs(60%)-MgO(40%)/EG
465 hybrid nanofluid by focusing on the thermal conductivity, Powder Technol. 342
466 (2019) 998-1007.
- 467 [2] M.H. Esfe, M. Goodarzi, M. Reiszadeh, M. Afrand, Evaluation of
468 MWCNTs-ZnO/5W50 nanolubricant by design of an artificial neural network
469 for predicting viscosity and its optimization, J. Mol. Liq. 277 (2019) 921-931.

- 470 [3] X. Liu, Y. Xuan, Full-spectrum volumetric solar thermal conversion via
471 photonic nanofluids, *Nanoscale* 9(39) (2017) 14854-14860.
- 472 [4] J. Zeng, Y. Xuan, Enhanced solar thermal conversion and thermal conduction of
473 MWCNT-SiO₂/Ag binary nanofluids, *Appl. Energ.* 212 (2018) 809-819.
- 474 [5] H.M. Ali, M.J. Ashraf, A. Giovannelli, M. Irfan, T.B. Irshad, H.M. Hamid, F.
475 Hassan, A. Arshad, Thermal management of electronics: an experimental
476 analysis of triangular, rectangular and circular pin-fin heat sinks for various
477 PCMs, *Int. J. Heat Mass Transf.* 123 (2018) 272-284.
- 478 [6] H.M. Ali, W. Arshad, Thermal performance investigation of staggered and inline
479 pin fin heat sinks using water based rutile and anatase TiO₂ nanofluids, *Energy*
480 *Convers. Manage.* 106 (2015) 793-803.
- 481 [7] M.M. Sarafraz, M. Arjomandi, Thermal performance analysis of a microchannel
482 heat sink cooling with Copper Oxide-Indium (CuO/In) nano-suspensions at
483 high-temperatures, *Appl. Therm. Eng.* 137 (2018) 700-709.
- 484 [8] L. Zhang, L. Fan, Z. Yu, R. Mei, Correlating convection heat transfer for
485 Falkner-Skan flow, *Int. J. Heat Mass Transf.* 131 (2019) 101-108.
- 486 [9] Y. Hu, H. Li, Y. He, Z. Liu, Y. Zhao, Effect of nanoparticle size and
487 concentration on boiling performance of SiO₂ nanofluid, *Int. J. Heat Mass*
488 *Transf.* 107 (2017) 820-828.
- 489 [10] A. Norouzipour, A. Abdollahi, M. Afrand, Experimental study of the optimum
490 size of silica nanoparticles on the pool boiling heat transfer coefficient of silicon
491 oxide/deionized water nanofluid, *Powder Technol.* 345 (2019) 728-738.

- 492 [11]M. Sheikholeslami, B. Rezaeianjouybari, M. Darzi, A. Shafee, Z. Li, T.K.
493 Nguyen, Application of nano-refrigerant for boiling heat transfer enhancement
494 employing an experimental study, *Int. J. Heat and Mass Transf.* 141 (2019)
495 974-980.
- 496 [12]M. Sheikholeslami, R.U. Haq, A. Shafee, Z. Li, Y.G. Elaraki, I. Tlili, Heat
497 transfer simulation of heat storage unit with nanoparticles and fins through a
498 heat exchanger, *Int. J. Heat and Mass Transf.* 135 (2019) 470-478.
- 499 [13]M. Sheikholeslami, R.U. Haq, A. Shafee, Z. Li, Heat transfer behavior of
500 nanoparticle enhanced PCM solidification through an enclosure with V shaped
501 fins, *Int. J. Heat and Mass Transf.* 130 (2019) 1322-1342.
- 502 [14]M. Sheikholeslami, M. Jafaryar, M. Hedayat, A. Shafee, Z. Li, T.K. Nguyen, M.
503 Bakouri, Heat transfer and turbulent simulation of nanomaterial due to
504 compound turbulator including irreversibility analysis, *Int. J. Heat and Mass
505 Transf.* 137 (2019) 1290-1300.
- 506 [15]B. Sun, A. Yang, D. Yang, Experimental study on the heat transfer and flow
507 characteristics of nanofluids in the built-in twisted belt external thread tubes, *Int.
508 J. Heat Mass Transf.* 107 (2017) 712-722.
- 509 [16]M. Sheikholeslami, M. Jafaryar, A. Ali, S.M. Hamad, A. Divsalar, A. Shafee, Z.
510 Li, Simulation of turbulent flow of nanofluid due to existence of new effective
511 turbulator involving entropy generation, *J. Mol. Liq.* 291 (2019) 111283.
- 512 [17]M. Sheikholeslami, M. Jafaryar, A. Shafee, Z. Li, R.U. Haq, Heat transfer of
513 nanoparticles employing innovative turbulator considering entropy

514 generation, *Int. J. Heat and Mass Transf.* 136 (2019) 1233-1240.

515 [18]C. Qi, M. Liu, J. Tang, Influence of triangle tube structure with twisted tape on
516 the thermo-hydraulic performance of nanofluids in heat-exchange system based
517 on thermal and exergy efficiency, *Energy Convers. Manage.* 192 (2019)
518 243-268.

519 [19]A. Karimi, A.A. Al-Rashed, M. Afrand, O. Mahian, S. Wongwises, A. Shahsavari,
520 The effects of tape insert material on the flow and heat transfer in a
521 nanofluid-based double tube heat exchanger: Two-phase mixture model, *Int. J.*
522 *Mech. Sci.* 156 (2019) 397-409.

523 [20]M. Sheikholeslami, A. Shafee, A. Zareei, R.U. Haq, Z. Li, Heat transfer of
524 magnetic nanoparticles through porous media including exergy analysis, *J. Mol.*
525 *Liq.* 279 (2019) 719-732.

526 [21]H. Xu, Z. Xing, K. Vafai, Analytical considerations of flow/thermal coupling of
527 nanofluids in foam metals with local thermal non-equilibrium (LTNE)
528 phenomena and inhomogeneous nanoparticle distribution, *Int. J. Heat Fluid*
529 *Flow* 77 (2019) 242-255.

530 [22]H. Xu, L. Gong, S. Huang, M. Xu, Flow and heat transfer characteristics of
531 nanofluid flowing through metal foams, *Int. J. Heat Mass Transf.* 83 (2015)
532 399-407.

533 [23]M. Sheikholeslami, New computational approach for exergy and entropy
534 analysis of nanofluid under the impact of Lorentz force through a porous
535 media, *Comput. Method. Appl. Mech. Eng.* 344, (2019) 319-333.

- 536 [24]P. Naphon, S. Wiriyasart, Pulsating flow and magnetic field effects on the
537 convective heat transfer of TiO₂-water nanofluids in helically corrugated
538 tube, *Int. J. Heat Mass Transf.* 125 (2018) 1054-1060.
- 539 [25]P. Naphon, S. Wiriyasart, T. Arisariyawong, L. Nakharintr, ANN, Numerical and
540 experimental analysis on the jet impingement nanofluids flow and heat transfer
541 characteristics in the micro-channel heat sink, *Int. J. Heat Mass Transf.* 131
542 (2019) 329-340.
- 543 [26]M. Izadi, M.M. Shahmardan, M. Norouzi, A.M. Rashidi, A. Behzadmehr,
544 Cooling performance of a nanofluid flow in a heat sink microchannel with axial
545 conduction effect, *Appl. Phys. A.* 117(4) (2014) 1821-1833.
- 546 [27]H. Babar, H.M. Ali, Towards hybrid nanofluids: preparation, thermophysical
547 properties, applications, and challenges, *J. Mol. Liq.* 281 (2019) 598-633.
- 548 [28]M. Sheikholeslami, Numerical investigation of nanofluid free convection under
549 the influence of electric field in a porous enclosure, *J. Mol. Liq.* 249 (2018)
550 1212-1221.
- 551 [29]M. Sheikholeslami, M. Seyednezhad, Simulation of nanofluid flow and natural
552 convection in a porous media under the influence of electric field using
553 CVFEM, *Int. J. Heat Mass Transf.* 120 (2018) 772-781.
- 554 [30]M. Sheikholeslami, M.K. Sadoughi, Simulation of CuO-water nanofluid heat
555 transfer enhancement in presence of melting surface, *Int. J. Heat Mass
556 Transf.* 116 (2018) 909-919.
- 557 [31]M. Sheikholeslami, S.A. Shehzad, Simulation of water based nanofluid

- 558 convective flow inside a porous enclosure via non-equilibrium model, *Int. J.*
559 *Heat Mass Transf.* 120 (2018) 1200-1212.
- 560 [32]M. Sheikholeslami, S.A. Shehzad, Z. Li, A. Shafee, Numerical modeling for
561 alumina nanofluid magnetohydrodynamic convective heat transfer in a
562 permeable medium using Darcy law, *Int. J. Heat Mass Transf.* 127 (2018)
563 614-622.
- 564 [33]M. Sheikholeslami, H.B. Rokni, Numerical simulation for impact of Coulomb
565 force on nanofluid heat transfer in a porous enclosure in presence of thermal
566 radiation, *Int. J. Heat Mass Transf.* 118 (2018) 823-831.
- 567 [34]M. Sheikholeslami, S.A. Shehzad, Numerical analysis of $\text{Fe}_3\text{O}_4\text{-H}_2\text{O}$ nanofluid
568 flow in permeable media under the effect of external magnetic source, *Int. J.*
569 *Heat Mass Transf.* 118 (2018) 182-192.
- 570 [35]M. Sheikholeslami, Z. Li, M. Shamlooei, Nanofluid MHD natural convection
571 through a porous complex shaped cavity considering thermal radiation, *Phys.*
572 *Lett. A* 382(24) (2018) 1615-1632.
- 573 [36]M. Sheikholeslami, Numerical approach for MHD $\text{Al}_2\text{O}_3\text{-water}$ nanofluid
574 transportation inside a permeable medium using innovative computer
575 method, *Comput. Method. Appl. Mech. Eng.* 344 (2019) 306-318.
- 576 [37]M. Sheikholeslami, S.A.M. Mehryan, A. Shafee, M.A. Sheremet, Variable
577 magnetic forces impact on magnetizable hybrid nanofluid heat transfer through a
578 circular cavity, *J. Mol. Liq.* 277 (2019) 388-396.
- 579 [38]M. Izadi, N.M. Maleki, I. Pop, S.A.M. Mehryan, Natural convection of a hybrid

580 nanofluid subjected to non-uniform magnetic field within porous medium
581 including circular heater, *Int. J. Numer. Method. Heat Fluid Flow* 29(4) (2019)
582 1211-1231.

583 [39]S.A.M. Mehryan, M. Izadi, Z. Namazian, A.J. Chamkha, Natural convection of
584 multi-walled carbon nanotube-Fe₃O₄/water magnetic hybrid nanofluid flowing
585 in porous medium considering the impacts of magnetic field-dependent
586 viscosity, *J. Therm. Anal. Calorim.* (2019)
587 <https://doi.org/10.1007/s10973-019-08164-1>

588 [40]A.H. Pordanjani, S. Aghakhani, A.A. Alnaqi, M. Afrand, Effect of alumina
589 nano-powder on the convection and the entropy generation of water inside an
590 inclined square cavity subjected to a magnetic field: Uniform and non-uniform
591 temperature boundary conditions, *Int. J. Mech. Sci.* 152 (2019) 99-117.

592 [41]A.H. Pordanjani, A. Jahanbakhshi, A.A. Nadooshan, M. Afrand, Effect of two
593 isothermal obstacles on the natural convection of nanofluid in the presence of
594 magnetic field inside an enclosure with sinusoidal wall temperature
595 distribution, *Int. J. Heat Mass Transf.* 121 (2018) 565-578.

596 [42]M. Izadi, H.F. Oztop, M.A. Sheremet, S.A.M. Mehryan, N. Abu-Hamdeh,
597 Coupled FHD-MHD free convection of a hybrid nanofluid in an inversed
598 T-shaped enclosure occupied by partitioned porous media, *Numer. Heat Transf.*
599 *Part A.* 76(6) (2019) 479-498.

600 [43]M. Izadi, R. Mohebbi, D. Karimi, M.A. Sheremet, Numerical simulation of
601 natural convection heat transfer inside a \perp shaped cavity filled by a

602 MWCNT-Fe₃O₄/water hybrid nanofluids using LBM, Chem. Eng. Process. 125
603 (2018) 56-66.

604 [44]M. Izadi, S. Sinaei, S.A.M. Mehryan, H.F. Oztop, N. Abu-Hamdeh, Natural
605 convection of a nanofluid between two eccentric cylinders saturated by porous
606 material: Buongiorno's two phase model, Int. J. Heat Mass Transf. 127 (2018)
607 67-75.

608 [45]M. Izadi, G. Hoghoughi, R. Mohebbi, M. Sheremet, Nanoparticle migration and
609 natural convection heat transfer of Cu-water nanofluid inside a porous
610 undulant-wall enclosure using LTNE and two-phase model, J. Mol. Liq. 261
611 (2018) 357-372.

612 [46]M. Izadi, R. Mohebbi, A.A. Delouei, H. Sajjadi, Natural convection of a
613 magnetizable hybrid nanofluid inside a porous enclosure subjected to two
614 variable magnetic fields, Int. J. Mech. Sci. 151 (2019) 154-169.

615 [47]M. Izadi, R. Mohebbi, A. Chamkha, I. Pop, Effects of cavity and heat source
616 aspect ratios on natural convection of a nanofluid in a C-shaped cavity using
617 Lattice Boltzmann method, Int. J. Numer. Method. Heat Fluid Flow 28(8) (2018)
618 1930-1955.

619 [48]H. Xu, Z. Xing, The lattice Boltzmann modeling on the nanofluid natural
620 convective transport in a cavity filled with a porous foam, Int. Commun. Heat
621 Mass Transf. 89 (2017) 73-82.

622 [49]M.R. Safaei, A. Karimipour, A. Abdollahi, T.K. Nguyen, The investigation of
623 thermal radiation and free convection heat transfer mechanisms of nanofluid

624 inside a shallow cavity by lattice Boltzmann method, *Physica A* 509 (2018)
625 515-535.

626 [50]M.A. Abbassi, M.R. Safaei, R. Djebali, K. Guedri, B. Zeghmami, A.A. Alrashed,
627 LBM simulation of free convection in a nanofluid filled incinerator containing a
628 hot block, *Int. J. Mech. Sci.* 144 (2018) 172-185.

629 [51]H. Goodarzi, O.A. Akbari, M.M. Sarafraz, M. Mokhtari, M.R. Safaei, G.A.S.
630 Shabani, Numerical simulation of natural convection heat transfer of nanofluid
631 with Cu, MWCNT and Al₂O₃ nanoparticles in a cavity with different aspect
632 ratios, *J. Therm. Sci. Eng. Appl.* 11(6) (2019) 061020.

633 [52]X. Zhou, Y. Jiang, X. Li, K. Cheng, X. Huai, X. Zhang, H. Huang, Numerical
634 simulation of natural convection heat transfer of nanofluid with Cu, MWCNT
635 and Al₂O₃ nanoparticles in a cavity with different aspect ratios, *Int. Commun.*
636 *Heat Mass Transf.* 106 (2019) 46-54.

637 [53]Y. Jiang, X. Zhou, Heat transfer and entropy generation analysis of nanofluids
638 thermocapillary convection around a bubble in a cavity, *Int. Commun. Heat*
639 *Mass Transf.* 105 (2019) 37-45.

640 [54]Y. Jiang, X. Zhou, Analysis of flow and heat transfer characteristics of
641 nanofluids surface tension driven convection in a rectangular cavity, *Int. J. Mech.*
642 *Sci.* 153 (2019) 154-163.

643 [55]S.A.M. Mehryan, M. Izadi, A.J. Chamkha, M.A. Sheremet, Natural convection
644 and entropy generation of a ferrofluid in a square enclosure under the effect of a
645 horizontal periodic magnetic field, *J. Mol. Liq.* 263 (2018) 510-525.

- 646 [56] Y. Ma, R. Mohebbi, M.M. Rashidi, Z. Yang, M.A. Sheremet, Numerical study of
647 MHD nanofluid natural convection in a baffled U-shaped enclosure, *Int. J. Heat*
648 *Mass Transf.* 130 (2019) 123-134.
- 649 [57] M.A. Sheremet, I. Pop, O. Mahian, Natural convection in an inclined cavity with
650 time-periodic temperature boundary conditions using nanofluids: application in
651 solar collectors, *Int. J. Heat Mass Transf.* 116 (2018) 751-761.
- 652 [58] I.V. Miroshnichenko, M.A. Sheremet, H.F. Oztop, N. Abu-Hamdeh, Natural
653 convection of alumina-water nanofluid in an open cavity having multiple porous
654 layers, *Int. J. Heat Mass Transf.* 125 (2018) 648-657.
- 655 [59] I.V. Miroshnichenko, M.A. Sheremet, H.F. Oztop, N. Abu-Hamdeh, Natural
656 convection of $\text{Al}_2\text{O}_3/\text{H}_2\text{O}$ nanofluid in an open inclined cavity with a
657 heat-generating element, *Int. J. Heat Mass Transf.* 126 (2018) 184-191.
- 658 [60] D.S. Bondarenko, M.A. Sheremet, H.F. Oztop, M.E. Ali, Natural convection of
659 $\text{Al}_2\text{O}_3/\text{H}_2\text{O}$ nanofluid in a cavity with a heat-generating element. Heatline
660 visualization, *Int. J. Heat Mass Transf.* 130 (2019) 564-574.
- 661 [61] N.S. Bondareva, M.A. Sheremet, H.F. Oztop, N. Abu-Hamdeh, Free convection
662 in an open triangular cavity filled with a nanofluid under the effects of Brownian
663 diffusion, thermophoresis and local heater, *ASME J. Heat Transf.* 140(4) (2018)
664 042502.
- 665 [62] F. Selimefendigil, H.F. Öztop, Mixed convection of nanofluids in a three
666 dimensional cavity with two adiabatic inner rotating cylinders, *Int. J. Heat Mass*
667 *Transf.* 117 (2018) 331-343.

- 668 [63]F. Selimefendigil, H.F. Öztop, Corrugated conductive partition effects on MHD
669 free convection of CNT-water nanofluid in a cavity, *Int. J. Heat Mass*
670 *Transf.* 129 (2019) 265-277.
- 671 [64]F. Selimefendigil, H.F. Öztop, Role of magnetic field and surface corrugation on
672 natural convection in a nanofluid filled 3D trapezoidal cavity, *Int. Commun.*
673 *Heat Mass Transf.* 95 (2018) 182-196.
- 674 [65]F. Selimefendigil, H.F. Öztop, Modeling and optimization of MHD mixed
675 convection in a lid-driven trapezoidal cavity filled with alumina-water nanofluid:
676 effects of electrical conductivity models, *Int. J. Mech. Sci.* 136 (2018) 264-278.
- 677 [66]F. Selimefendigil, H.F. Öztop, Conjugate mixed convection of nanofluid in a
678 cubic enclosure separated with a conductive plate and having an inner rotating
679 cylinder, *Int. J. Heat Mass Transf.* 139 (2019) 1000-1017.
- 680 [67]R. Mohebbi, M. Izadi, H. Sajjadi, A.A. Delouei, M.A. Sheremet, Examining of
681 nanofluid natural convection heat transfer in a Γ -shaped enclosure including a
682 rectangular hot obstacle using the lattice Boltzmann method, *Physica A.* 526
683 (2019) 120831.
- 684 [68]H. Sajjadi, A.A. Delouei, M. Izadi, R. Mohebbi, Investigation of MHD natural
685 convection in a porous media by double MRT lattice Boltzmann method
686 utilizing MWCNT-Fe₃O₄/water hybrid nanofluid, *Int. J. Heat Mass Transf.* 132
687 (2019) 1087-1104.
- 688 [69]R. Mohebbi, S.A.M. Mehryan, M. Izadi, O. Mahian, Natural convection of
689 hybrid nanofluids inside a partitioned porous cavity for application in solar

690 power plants, *J. Therm. Anal. Calorim.* 137 (2019) 1719-1733.

691 [70]C. Qi, L. Liang, Z. Rao, Study on the flow and heat transfer of liquid metal base
692 nanofluid with different nanoparticle radiuses based on two-phase lattice
693 Boltzmann method, *Int. J. Heat Mass Transf.* 94 (2016) 316-326.

694 [71]C. Qi, G. Wang, L. Yang, Y. Wan, Z. Rao, Two-phase lattice Boltzmann
695 simulation of the effects of base fluid and nanoparticle size on natural
696 convection heat transfer of nanofluid, *Int. J. Heat Mass Transf.* 105 (2017)
697 664-672.

698 [72]Y. Hu, Y. He, C. Qi, B. Jiang, H.I. Schlaberg, Experimental and numerical study
699 of natural convection in a square enclosure filled with nanofluid, *Int. J. Heat*
700 *Mass Transf.* 78 (2014) 380-392.

701 [73]C. Qi, Y.L. Wan, G.Q. Wang, D.T. Han, Study on stabilities, thermophysical
702 properties and natural convective heat transfer characteristics of TiO₂-water
703 nanofluids, *Indian J. Phys.* 92(4) (2018) 461-478.

704 [74]S. Mei, C. Qi, M. Liu, F. Fan, L. Liang, Effects of paralleled magnetic field on
705 thermo-hydraulic performances of Fe₃O₄-water nanofluids in a circular tube, *Int.*
706 *J. Heat Mass Transf.* 134 (2019) 707-721.